To access the final edited and published work is available online at https://doi.org/10.1364/JOSAB.35.001295

Coexistence of two-photon absorption and saturable absorption in ion-implanted platinum nanoparticles in silica plates

C. Torres-Torres,[1*] J. Bornacelli,[2] B. Can-Uc,[3] H. G. Silva-Pereyra,[4] L. Rodríguez-Fernández,[2] M. Avalos-Borja,[4] J. C. Cheang-Wong,[2] R. Rangel-Rojo,[5] and A. Oliver[2]

[1]Sección de Estudios de Posgrado e Investigación, Escuela Superior de Ingeniería Mecánica y Eléctrica Unidad Zacatenco, Instituto Politécnico Nacional, Ciudad de México, 07738, México

[2]Instituto de Física, Universidad Nacional Autónoma de México, Ciudad de México, 04510, México

[3]Centro de Nanociencias y Nanotecnología, Universidad Nacional Autónoma de México, A. P. 14, Ensenada, B.C., 22800, México

[4]IPICyT, División de Materiales Avanzados, Camino a la Presa San José 2055, San Luis Potosí, San Luis Potosí, 78216, México

[5]Depto. de Óptica, Centro de Investigación Científica y de Educación Superior de Ensenada A.P. 360, Ensenada, B.C., 22860, México

---

*Corresponding author: Carlos Torres-Torres

Email: ctorrest@ipn.mx; crstorres@yahoo.com.mx

Sección de Estudios de Posgrado e Investigación, Escuela Superior de Ingeniería Mecánica y Eléctrica Unidad Zacatenco, Instituto Politécnico Nacional, Ciudad de México, 07738, México. Phone +52(55)57-29-60-00, ext. 54686

Abstract

Platinum nanoparticles were nucleated in a high purity silica matrix by an ion-implantation method. The third-order nonlinear optical response of the samples was studied using femtosecond pulses at 800 nm with the z-scan technique; picosecond pulses at 532 nm using a self-diffraction approach; and nanosecond pulses at 532 nm employing a vectorial two-wave mixing experiment. Nanosecond and picosecond explorations indicated an important thermal process participating in the optical Kerr effect evaluated. However, femtosecond results allowed us to distinguish a purely electronic response, related exclusively to ultrafast refractive and absorptive nonlinearities. Femtosecond experiments pointed out the possibility to switch the dominant physical mechanism responsible for the nonlinear optical absorption in the sample. This opens the potential for controlling quantum mechanisms of optical nonlinearity by femtosecond interactions.

Keyword: Nonlinear Optics; metallic nanoparticles, ion-implantation; Surface Plasmon Resonance.

1. Introduction

Current trends in the development of low-dimensional systems have been importantly shaped by the convergence between ultrafast functions and nanotechnology. Modern integration of a large variety of nanostructures has provided revolutionary possibilities for the progress of nonlinear optics and materials science [1]. Metallic nanoparticles (NPs) are attractive for biomedical and telecom applications in regards to their fascinating and selective effects

ordinarily associated with their Surface Plasmon Resonance (SPR) [2]. Plasmonic NPs can be synthesized with specific shape and size according to diverse chemical or physical methods that open up possibilities for engineering multidisciplinary applications [3]. It is remarkable that ion-implantation techniques are particularly useful for designing micro- and nano-electronic devices taking into account their potential for preparing nanoparticle distributions systematically controlled by MeV energies and irradiation conditions [4,5]. Platinum NPs (PtNPs) mainly differ from other important noble metal NPs because of their unique SPR absorption band located in the ultraviolet region of the electromagnetic spectrum, [6] yielding composites that are transparent throughout the visible. Chemical stability and high melting temperature of PtNPs have motivated for manufacturing these nanomaterials to enhance the sensitivity of advanced detectors [7]. Besides, the powerful photocatalytic activity related to PtNPs makes them suitable for both sensing and instrumentation of other elements in nanobiomedicine [8]. The capability of quantum confinement of ultraviolet energy by the SPR action exhibited by PtNPs can be an important advantage to design single-photon devices [9]. Third-order nonlinear optical phenomena that concern to the PtNPs behavior seem to be strong enough for future prospects that include all-optical operations [10], sensing mechanisms [11], tracking tools in medicine and biology [12], and waveguiding [13]; among other applications. With these considerations, quantum interactions related to high-energy photons driven by PtNPs can be also envisioned to play a key role in measurement and information processing [14]. Here we report an attempt to further explain the off-resonance nonlinear optical behaviors exhibited by PtNPs. The ion-implanted samples were nucleated in high-purity silica plates. In order to investigate the absorptive and refractive optical nonlinearities of the nanocomposites, third-order nonlinear optical measurements were undertaken by using nano-, pico- and femto-second pulses. The

combination of high transparency, and large nonlinear response of these PtNPs composites makes them attractive for all-optical signal processing applications.

2. Experimental

2.1. Sample preparation

PtNPs were prepared by ion-implantation using the 3MV Tandem accelerator (NEC 9SDH-2 Pelletron) facility at the Instituto de Física of the Universidad Nacional Autónoma de México [15]. A high-purity Silica substrate (suprasil 300) was implanted as a matrix exposed to 1.9 MeV Pt ions with a fluence of $1.11x10^{16}$ Pt/cm^2. A thermal annealing process after implantation was carried out in the as-implanted sample with 600°C in a reducing atmosphere based on Nitrogen. By using Rutherford Backscattering Spectrometry (RBS) with 2MeV $^4He^{++}$ beam, the concentration and depth profile of the implanted Pt in the sample was measured. Nanoscopic studies were performed by the assistance of a FEI TECNAI F30 Transmission Electron Microscope (FEG-TEM 300kV) in scanning mode (STEM) with a HAADF detector (Z-contrast). Spectroscopic evaluations were conducted with a Varian Cary 5000 UV-VIS spectrophotometer. All the setups for nonlinear optical measurements were previously calibrated with a standard CS_2 sample contained in a quartz cuvette with 1 mm of optical path.

2.2. Femtosecond z-scan experiments

A Ti:sapphire laser system with λ =800 nm, 80 fs pulses, and a repetition rate at 94 MHz was employed to study the third-order nonlinear optical parameters by the z-scan technique [16]. The pulses were focused with a lens to produce a Gaussian beam with a 47 μm waist Full Width Half Maximum (FWHM) that was employed in both the open- and closed-aperture

configurations of the z-scan. In the open-aperture z-scan, a detector located in the far-field measures the transmittance of the sample, as its position is scanned through the focal plane of the beam. Since the irradiance changes with sample position z, the technique will detect changes in transmittance due to nonlinear absorption. For the closed-aperture z-scan, an aperture is now placed in front of the detector, so that curvature chances in the beam, induced by nonlinear refraction in the sample, can be translated into transmittance changes. In this way, the closed-aperture z-scan is sensitive to nonlinear refraction, although it is still sensitive to nonlinear absorption if it is present in the sample. The normalized transmittance as function of sample position z for the open z-scan measurements can be approximately written as [16]:

$$T\left(z,\Delta\Phi_o\right)=1-\frac{\beta I_o L_{eff}}{2\sqrt{2}\left(x^2+1\right)}\ , \tag{1}$$

where β represents the nonlinear optical absorption coefficient, and L_{eff} is the effective length given by $L_{eff}=(1-e^{-\alpha_0 L})/\alpha_0$, where L is the actual sample thickness, and α_o is the linear absorption coefficient.

In a similar way, for a Gaussian beam with waist radius w_o, the normalized transmittance T through the aperture, also as function of sample position z, in terms of the on-axis nonlinear phase $\Delta\Phi_o$, can be approximately written as [16]:

$$T\left(z,\Delta\Phi_o\right)=1-\frac{4\Delta\Phi_o x}{\left(x^2+9\right)\left(x^2+1\right)}\ , \tag{2}$$

with $x=z/z_o$, $z_o=kw_o^2/2$ $k=2\pi/\lambda$, and λ the laser wavelength, all in free space. In addition, the peak nonlinear phase change $\Delta\Phi_0$ is given by:

$$\Delta\Phi_o=k\Delta n_o L_{eff}\ , \tag{3}$$

here $\Delta n_0 = n_2 I_0$ represents the on-axis maximum refractive index change, where n_2 is the nonlinear refractive index, and I_0 is the peak on-axis irradiance at focus.

2.3. Picosecond self-diffraction measurements

A degenerated two-wave mixing experiment was used to identify the physical mechanism responsible for the nonlinear refractive index [17]. The second harmonic emerging from a Nd:YAG laser system (EKSPLA) with pulse duration of 25 ps was the optical source for performing the measurements. The incident probe and pump beams at 532 nm wavelength were linearly polarized and adjusted to present an irradiance relation of 1:2. These beams were focused on the sample with their propagation direction making an angle θ of 10°, had a spot size close to 0.1 mm with total incident pulse energy of 55 μJ, at a 1 Hz repetition rate. The polarization of the probe beam was fixed while the polarization of the pump beam was rotated by using a half-wave plate. As a consequence of the interaction, two self-diffracted beams are produced going in the forward direction, at angles θ outside of each incident beam direction. The self-diffracted energies were acquired by using a PIN photodetector.

The approximate amplitudes of the transmitted, and self-diffracted fields were calculated considering [17]:

$$\nabla^2 E_{\pm} = -\frac{n_{\pm}^2 \omega^2}{c^2} E_{\pm} \tag{4}$$

where the right and left circular components of the electric field are E_+ and E_- ; respectively. The optical frequency is ω and the refractive index was approximated [17]

$$n_{\pm}^2 = n_0^2 + 4\pi \left(A \left| E_{\pm} \right|^2 + (A + B) \left| E_{\mp} \right|^2 \right) \tag{5}$$

where $A = \chi^{(3)}_{1122}$ and $B = \chi^{(3)}_{1212}$ are the elements of the third-order susceptibility tensor, and n_0 is the weak-field refractive index.

2.4. Nanosecond Optical Kerr Gate evaluations

Similarly to the picosecond experiments, nanosecond experiments were carried out by using a two-wave mixing configuration. However, since nanosecond irradiances may produce ablation before the observation of a self-diffraction effect, in this case we just analyzed the modification of the polarization of the probe beam by the induced birefringence originated by a pump beam in an Optical Kerr Gate experiment [17]. The 532 nm pulses provided by the second harmonic of a Nd-YAG laser system (Continuum Model SL II) with 4 ns pulse duration were employed as the optical source for the nanosecond nonlinear optical experiments. The probe and pump beams were linearly polarized and they had their propagation vectors making a 15^o angle. The maximum energy of the pump beam was 75 mJ per pulse and the probe beam was represented by a 10 nJ pulse. The initial beam waist for the pump and probe beams corresponded to 6 mm and 1 mm; respectively. The polarized irradiance of the probe-beam transmitted in the optical Kerr gate was measured with a PIN photodetector after the orthogonal component of the transmitted polarization passed through an analyzer. The third-order optical susceptibility was estimated for different conditions of focused pump beam taking into account the irradiances that correspond to the linear polarization components of the electric field described by Eq. (4).

3. Results and Discussions

3.1. Nanoparticle characterization

RBS results revealed that the Pt distribution in the sample correspond to a Gaussian profile. The location of the Pt implanted ions can be associated to a spatial region confined in an interval of about 700 nm with a peak in about 650 nm from the silica surface. The FWHM of the profile distribution was estimated to be extended approximately 200 nm.

Figure 1a shows a TEM image of the sample. The bright points represent the ion-implanted PtNPs with an approximated average size close to 1 nm. Figure 1b illustrates the UV-vis spectrum of the sample studied. The fit was performed by using the Mie theory with a standard deviation σ= 0.3 nm and the average diameter of the NPs <D> = 1.2 nm. From the absorbance data plotted can be clearly observed that the nanocomposites are quite transparent in the visible region of the spectrum and their maximum absorption takes place in the UV region of the spectrum. The peak of the absorption band of the SPR of the PtNPs can be usually detected near 280 nm; in our graph there is just a slight modulation of the curve below 300 nm; it could be a consequence derived from the small size of the NPs as it has been previously reported [15].

[Figure 1]

3.2. Femtosecond z-scan studies at 800 nm

The open-aperture results obtained using femtosecond pulses at 800 nm for two different irradiances, 44 and 109 MW/cm^2, are shown in Fig 2a, and Fig. 2b, respectively. In both cases the presence of two different nonlinear absorption mechanisms can be clearly seen: for

low irradiance values, *i.e.* sample positions away from the focal plane, the transmittance decreases, indicating that an induced (or reverse saturable) absorption process (such as two-photon absorption for example) is present. For positions near the focal plan ($z \approx 0$) the transmittance increases, the indication of a saturable absorption process, so the nonlinear response is a combination of the two processes.

[Figure 2]

This behavior of the open aperture transmittance cannot be properly modeled by the conventional theory resulting in expression (1) [16] for obtaining the nonlinear optical absorption coefficient. For such a case, with two superimposed processes, the theory proposed in reference [18] can be used, where they have considered the following equation for the nonlinear absorption coefficient β:

$$\beta(I) = \beta_{RSA}(I) + \beta_{SA}(I) = \frac{\beta_{RSA}}{1+\frac{I}{I_s^{RSA}}} + \frac{\beta_{SA}}{1+\frac{I}{I_s^{SA}}}, \tag{7}$$

where β_{RSA} and β_{SA} represent the reverse saturable absorption (RSA) coefficient ($\beta > 0$), and the saturable absorption (SA) coefficient ($\beta < 0$), respectively. The values I_s^{RSA} and I_s^{SA} represent the saturation intensities of both nonlinear optical absorption processes. Herein, the values used to generate the best fitted curve in Fig. 2a and 2b, are presented in **Table 1.**

Table 1 Optical parameters to fitted curves for the femtosecond nonlinear absorption processes.

I_s^{SA} (W/cm^2)	$(2 \pm 0.2) \times 10^7$
I_s^{RSA} (W/cm^2)	$(1.2 \pm 0.12) \times 10^7$
β_{SA} (cm/W)	$(-9.69 \pm 2.21) \times 10^{-5}$
β_{RSA} (cm/W)	$(14.355 \pm 0.3) \times 10^{-5}$
$\beta(I)$ (cm/W)	$(4.6650 \pm 0.8) \times 10^{-5}$

The closed aperture z-scan results at the same irradiances are shown in Fig. 2c for a 44 MW/cm^2 irradiance, and in Fig. 2d for 109 MW/cm^2. In both cases, the signature of a positive nonlinear refractive index n_2 can be clearly seen, a pre-focal ($z<0$) transmittance minimum followed by a post-focal ($z>0$) transmittance maximum. The actual transmittance change measured is quite small; nevertheless discernable with a good signal-to-noise ratio. Given the very small transmittance changes measured, the fit to the closed-aperture results is made using the usual irradiance dependence for the refractive index n:

$$n(I)=n_0+n_2 I, \tag{8}$$

where n_0 is the linear refractive index, and n_2 is the nonlinear refractive index introduced in (3), which is proportional to $\mathrm{Re}\chi^{(3)}$. In this case, we can use expression (2) to perform the fitting. Fitting the data at both irradiances results in $n_2=(6.41 \pm 0.75)\times 10^{-11}$cm^2/W, where the error estimation stems from the differences in the fits for each irradiance.

In this case, since linear absorption at the laser wavelength is negligible, this response can be explained by a two-photon absorption process dominant at lower irradiances, followed by excited-state absorption by the carriers created by two-photon absorption, that becomes important for higher irradiances. It is an interesting feature being able to shift from one process to the other by changing the input irradiance. The n_2 value determined is five orders

of magnitude larger than that of silica (3.2×10^{-16} cm^2/W [17]), which combined with its transparency in the visible, makes it interesting for all-optical switching applications.

3.3. Picosecond two-wave mixing with self-diffraction at 532 nm

The results for the picosecond two-wave mixing experiments are shown in Fig. 3, which plots the forward self-diffracted signal as a function of the angle between the polarizations of the two beams. The reproducibility of the data was corroborated by the exploration of different regions studied in two comparative samples fabricated by similar conditions of preparation. The results show the signature of a thermal nonlinearity, a self-diffracted signal that goes to zero for θ=90°, i.e. for the case when both polarizations are orthogonal to each other [20]. In this case, the interference of the two beams does not produce either an absorption or refractive index grating, but rather a polarization modulation. A thermal response will not result in an induced birefringence, and thus the self-diffractive signal for θ=90° will be negligible. The absence of a signal in the experimental results at this angle, indicates then that the only significant component of the response observed is thermal in origin. Figure 3 shows the fit to the data made using expressions (4) and (5), and from which the value of the third-order nonlinear optical susceptibility value $\left|\chi_{eff}^{(3)}\right| = 2.9 \times 10^{-10} esu$ was extracted.

[Figure 3]

3.4. Nanosecond Optical Kerr Gate at 532 nm

In order to comparatively analyze the picosecond nonlinear optical response at 532 nm by a different pulse duration interaction, nanosecond experiments were undertaken and the results

are shown in Fig. 4. The transmitted probe irradiance in the plot of Fig. 4 corresponds to Optical Kerr Gate measurements. In absence of a pump beam, a null transmitted probe signal is detected in this experiment; however Fig. 4 illustrates that is possible to generate a modulation of the polarization of the probe beam that can be detected as a function of the polarization of the pump beam in propagation through the sample. When the planes of polarization of pump and probe beam are parallel or orthogonal (0 ^{o} and 90^{o} in the plot; respectively), the induced refraction just generates changes of phase in the probe signal but no modification in polarization. The smooth and highly symmetric vectorial behavior exhibited by the sample points to a homogeneous distribution of the quasi-spherical NPs in the sample as it was confirmed by spectroscopic measurements monitoring the absorption spectrum for the sample in geometrical rotation. Each point in the plot is related to the average of 20 laser shots. The magnitude of $\left|\chi_{eff}^{(3)}\right| = 3.17\times10^{-9} esu$ was calculated for the nanosecond regime by using Eqs. (4) and (5). The $\left|\chi_{eff}^{(3)}\right|$ value obtained by nanosecond pulses is approximately one order of magnitude higher that the same parameter for picosecond pulses that may be explained by considering a different contribution of a thermal mechanism for the nonlinear refraction at different pulse duration.

[Figure 4]

Considering that the third-order nonlinear optical response of Silica can be negligible in comparison to the PtNPs contribution, it is assumed that the evolution of the third-order nonlinear optical behavior can be attributed to the exclusive participation of the PtNPs. It has been previously reported that plasmonic effects can give origin to an important enhancement of the nonlinear optical response of the material [21]. Moreover, it is well-known that laser induced nonlinear excitation of collective electron motion also produce the

possibility to improve optical effects [22]. Cooperative nonlinear optical properties of disordered plasmonic materials also involve the modification of the optical and physical behavior [23]. Regarding the versatility of PtNPs to present different mechanism of optical nonlinearity under fast and ultrafast pulses, we contemplate the possibility to use Pt nanocomposites as a platform for developing diverse all-optical functions.

4. Conclusions

The cooperative third-order nonlinear optical response exhibited by ion-implanted PtNPs in Silica was analyzed for nano-, pico-, and femto-second pulses. The dominant mechanism responsible for the nonlinear optical absorption in the sample seems to be sensitive to the femtosecond irradiation conditions. Picosecond self-diffraction results confirmed an important contribution of thermal effects for the nano- and pico-second optical Kerr effects observed. Femto-second z-scan results allowed us to distinguish the evolution of the electronic behavior of the third-order optical nonlinearities from saturated absorption to two-photon absorption with dependence on the irradiance conditions. Taking into account the possibility to control the ultrafast optical absorption in a quantic fashion, potential applications for developing all-optical discrete operations in Pt nanostructured systems can be contemplated.

Acknowledgements

The authors kindly acknowledge the financial support from CICESE, Instituto Politécnico Nacional through grant SIP20170498, Universidad Nacional Autónoma de México through grant DGAPA-UNAM IN108217, and from CONACyT through grants 222485 and CB-2015-251201. B. Can-Uc acknowledges the Posdoctoral Scholarship provided by DGAPA-UNAM. We wish to acknowledge to K. Lopez and F.J. Jaimes for running the accelerator

and J.G. Morales for his assistance during the sample preparation. The authors also acknowledge to the Laboratory for Nanoscience and Nanotechnology Research-LINAN of IPICYT for STEM characterization facilities.

5. References

[1] Anton Frisk Kockum, Adam Miranowicz, Vincenzo Macrì, Salvatore Savasta, and Franco Nori. Deterministic quantum nonlinear optics with single atoms and virtual photons. Phys. Rev. A 95, 063849, 2017.

[2] Xie Tao, Jing Chao, Long Yi-Tao. Single plasmonic nanoparticles as ultrasensitive sensors. Analyst, 142(3) 409- 420, 2017.

[3] A. Genç, J. Patarroyo, J. Sancho-Parramon, Neus G Bastus, V. Puntes, J Arbiol. Hollow metal nanostructures for enhanced plasmonics: synthesis, local plasmonic properties and applications. Nanophotonics, 6(1), 193-213, 2016.

[4]Yann Battie, Aotmane En Naciri, Nouari Chaoui, Yann Le Gall, Dominique Muller, Marzia Carrada, and Daniel Mathiot. Plasmonic properties of implanted Ag nanoparticles in SiO_2 thin layer by spectroscopic ellipsometry. Journal of Applied Physics, 122, 085308, 2017.

[5] Ovidio Peña-Rodríguez, Alejandro Prada, José Olivares, Alicia Oliver, Luis Rodríguez-Fernández, Héctor G. Silva-Pereyra, Eduardo Bringa, José Manuel Perlado, Antonio Rivera. Understanding the ion-induced elongation of silver nanoparticles embedded in silica. Scientific Reports 7, Article number: 922, 2017.

[6] G. Barcaro, L. Sementa, A. Fortunelli and M. Stener. Optical Properties of Pt and Ag−Pt Nanoclusters from TDDFT Calculations: Plasmon Suppression by Pt Poisoning J. Phys. Chem. C 118 28101-8, 2014.

[7] C. Zhang, X. Shen, Y. Pan, and Z. Peng. A review of Pt-based electrocatalysts for oxygen reduction reaction. Frontiers in Energy, 1-18, 2017.

[8] J. Wu, and H. Yang. Platinum-based oxygen reduction electrocatalysts. Accounts of chemical research, 46(8), 1848-1857, 2013.

[9] R. A. Ganeev, M. Suzuki, M. Baba, M. Ichihara, and H. Kuroda, Low-and high-order nonlinear optical properties of Au, Pt, Pd, and Ru nanoparticles. Journal of Applied Physics, 103(6), 063102, 2008.

[10] M. H. Mezher, W. Y. Chong and R. Zakaria, Nonlinear optical response of platinum nanostructures and application for water detection in transformer oil, RSC Adv., 6, 104624, 2016.

[11] N. H. Ha, C. T. Long, N. H. Nam, N. T. Hue, N. H. Phuong, and H. S. Hong. Characteristics of Hydrogen Sensor Based on Monolayer of Pt Nanoparticles Decorated on Single-Layer Graphene. Journal of Electronic Materials, 46(6), 3353-3358, 2017.

[12] A. Sápi, A. Kéri, I. Kálomista, D. G. Dobó, Á. Szamosvölgyi, K. L. Juhász, Á. Kukovecz, Z. Kónya and G. Galbács. Determination of the platinum concentration of a Pt/silica nanocomposite decorated with ultra small Pt nanoparticles using single particle inductively coupled plasma mass spectrometry. Journal of Analytical Atomic Spectrometry, 32(5), 996-1003, 2017.

[13] B. Can-Uc, R. Rangel-Rojo, A. Pena-Ramírez, C. B. de Araujo, H. T. M. C. M. Baltar, A. Crespo-Sosa, M. L. Garcia-Betancourt, and A. Oliver. Nonlinear optical response of platinum nanoparticles and platinum ions embedded in sapphire. Opt. Express 24 9955-9965, 2016.

[14] Stepanov Andrey, Golubev Andrey, Nikitin Sergey, Synthesis and Applications of Platinum Nanoparticles: A Review, In book: Nanotechnology Vol. 2: Synthesis and

Characterization, Chapter: Synthesis and Applications of Platinum Nanoparticles: A Review, 173-199, 2013.

[15] Jhovani Bornacelli, Carlos Torres-Torres, Héctor Gabriel Silva-Pereyra, Luis Rodríguez-Fernández, Miguel Avalos-Borja, Juan Carlos Cheang-Wong and Alicia Oliver. Nanoscale influence on photoluminescence and third order nonlinear susceptibility exhibited by ion-implanted Pt nanoparticles in silica. Methods Appl. Fluoresc. 5, 025001, 2017.

[16] M. Sheik-Bahae, A. A. Said, T. Wei, D. J. Hagan, E. W. V. Stryland. Sensitive measurement of optical nonlinearities using a single beam. IEEE J. Quantum Electron., 26, 760-769, 1990.

[17] R. W. Boyd. Nonlinear optics; 3rd. ed.; Academic Press: San Diego, 2008.

[18] T. Cesca, P. Calvelli, G. Battaglin, P. Mazzoldi, and G. Mattei. Local-field enhancement effect on the nonlinear optical response of gold-silver nanoplanets. Opt. Express**,** 20(4) 4537-4547, 2012.

[19] R. Rangel-Rojo, S. Yamada, H. Matsuda, H. Kasai, H. Nakanishi, A. K. Kar, and B. S. Wherrett. Spectrally resolved third-order nonlinearities in polydiacetylene microcrystals: influence of particle size. J. Opt. Soc. Am. B 15, 2937-2945, 1998.

[20] C. Torres-Torres, A. V. Khomenko, J. C. Cheang-Wong, A. Crespo-Sosa, L. Rodríguez-Fernández, A. Oliver. Absorptive and refractive nonlinearities by four wave mixing in Au nanoparticles in ion-implanted silica. Opt. Express, 15, 9248-9253, 2007.

[21]J. B. Khurgin and G. Sun, Plasmonic enhancement of the third order nonlinear optical phenomena: figures of merit. Opt. Express 21(22), 27460–27480, 2013.

[22] S. V. Fomichev, S. V. Popruzhenko, D. F. Zaretsky and W. Becker. Laser-induced nonlinear excitation of collective electron motion in a cluster. Journal of Physics B: Atomic, Molecular and Optical Physics, 36(18), 3817, 2003.

[23] F. J. Diaz, T. Hatakeyama, J. Rho, Y. Wang, K. O'Brien, X. Zhang, C. Martijn de Sterke, B. T. Kuhlmey, and S. Palomba. Sensitive method for measuring third order nonlinearities in compact dielectric and hybrid plasmonic waveguides. Opt. Express**,** 24(1) 545-554, 2016.

Figure Captions

Figure 1. (a) TEM image of the ion-implanted PtNPs embedded in Silica. (b) UV-vis spectrum of the sample.

Figure 2. Femtosecond z-scan results at 825 nm in PtNPs embedded in Silica (a) open aperture configuration 44 MW/cm^2 (b) open aperture configuration 109 MW/cm^2 (c) closed aperture configuration 44 MW/cm^2 (d) closed aperture configuration 109 MW/cm^2. The

experimental data are plotted as marks while the numerical fits are presented through solid lines.

Figure 3. Picosecond self-diffraction vs angle of polarization of the interacting beams in the samples studied.

Figure 4. Nanosecond nonlinear optical probe transmittance vs angle of polarization of the interacting beams in the samples studied by an optical Kerr gate.

Figure 1a

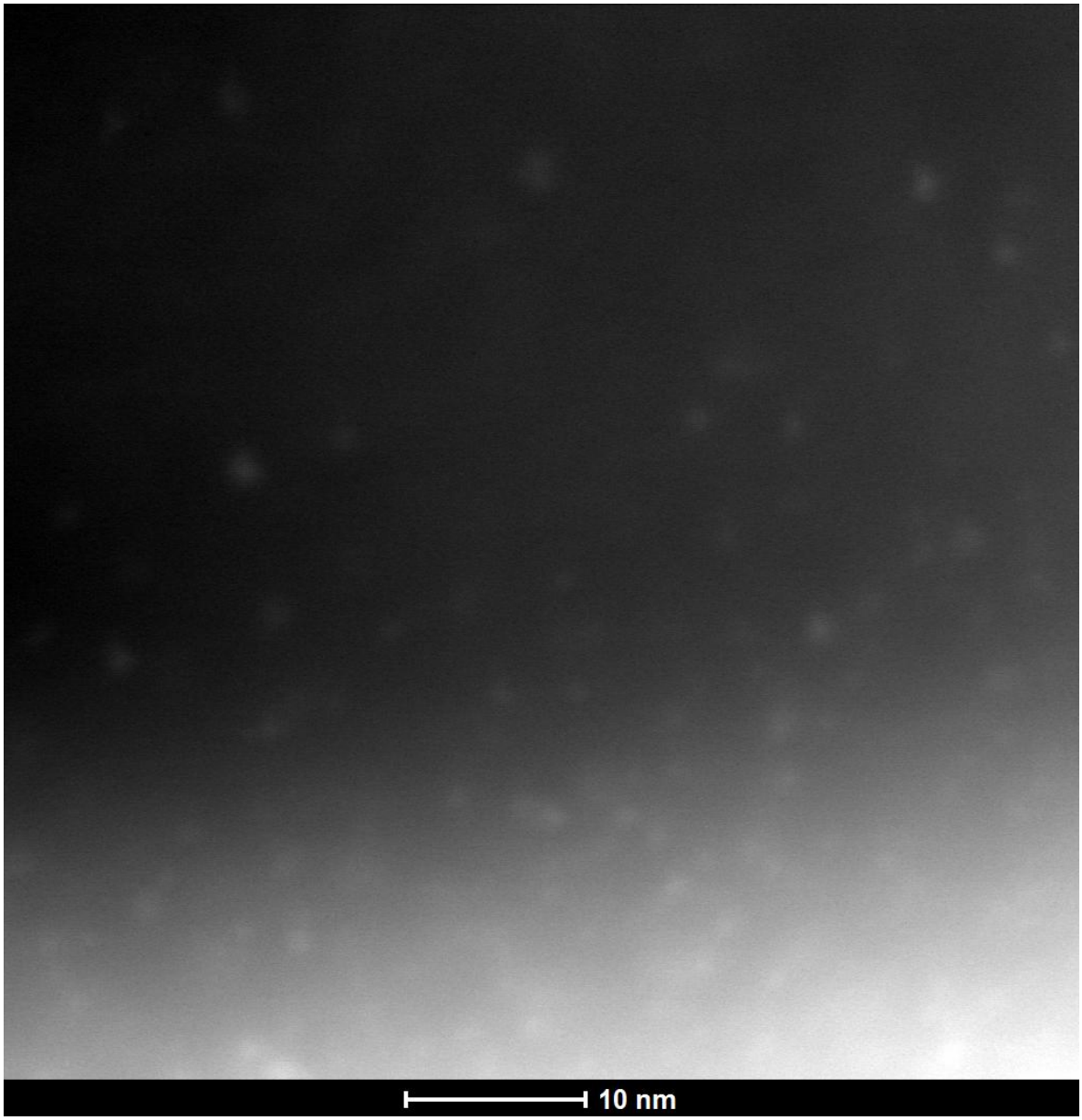

Figure 1b

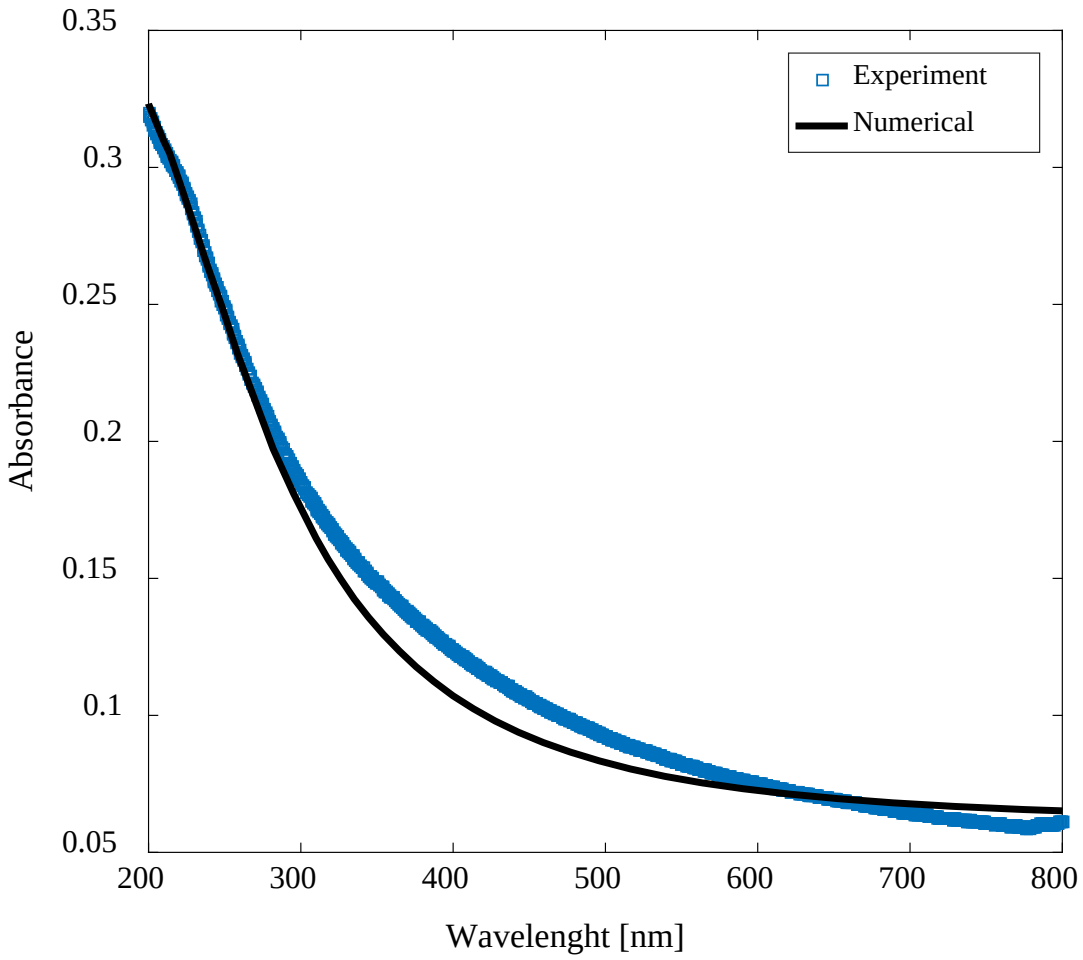
Experiment
Numerical
Absorbance
Wavelenght [nm]
0.35
0.3
0.25
0.2
0.15
0.1
0.05
200
300
400
500
600
700
800

Figure 2a

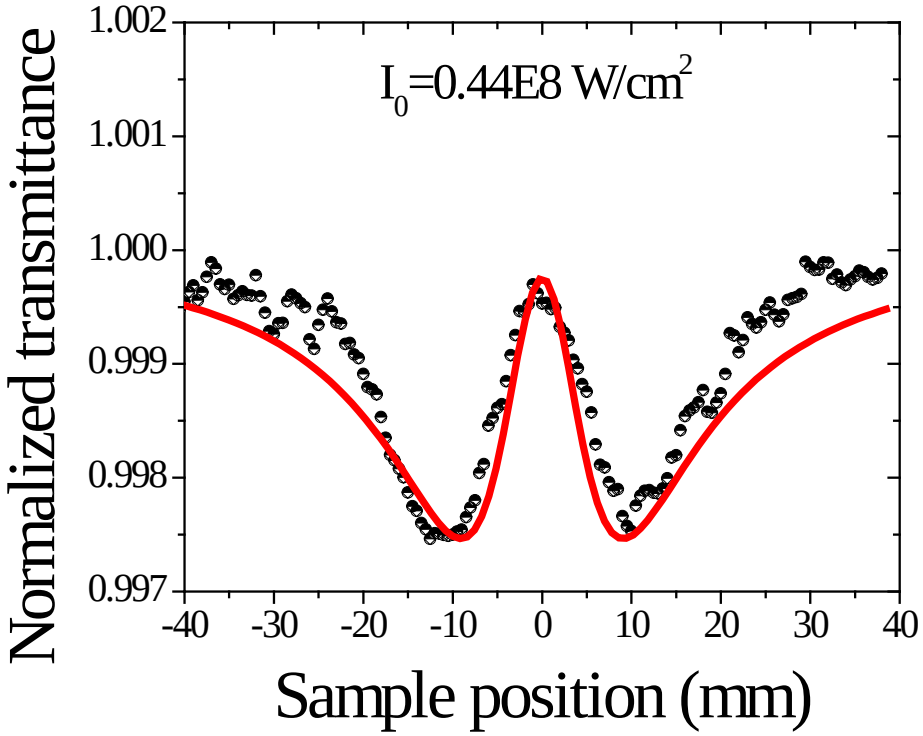
Normalized transmittance
1.002
1.001
1.000
0.999
0.998
0.997
I_0=0.44E8 W/cm^2
-40
-30
-20
-10
0
10
20
30
40
Sample position (mm)

Figure 2b

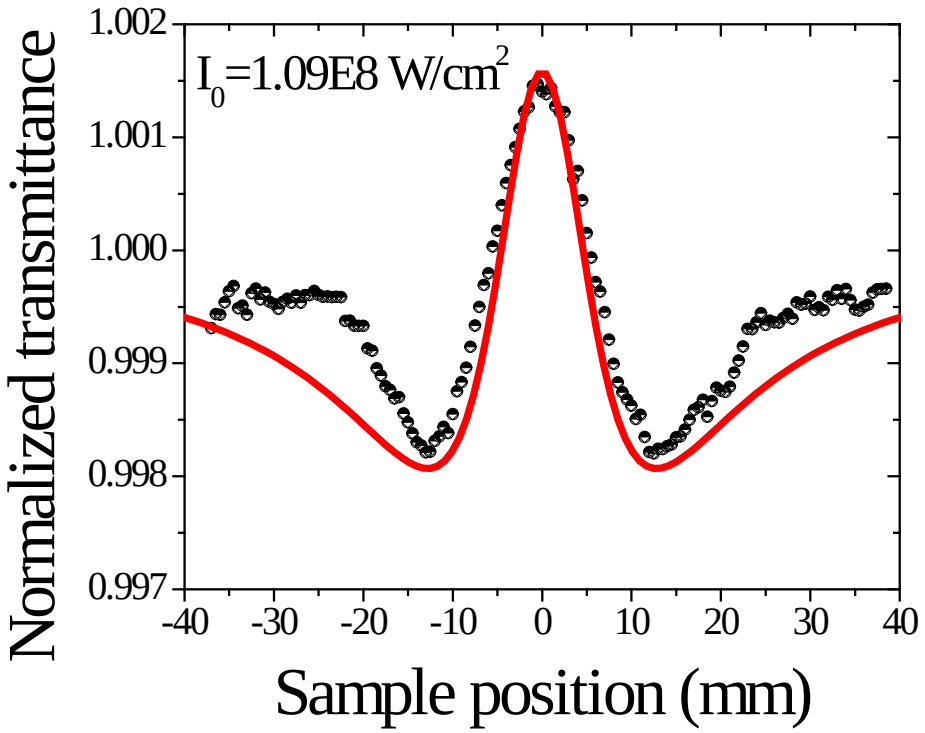
Normalized transmittance
Sample position (mm)
I0=1.09E8 W/cm2
1.002
1.001
1.000
0.999
0.998
0.997
-40
-30
-20
-10
0
10
20
30
40

Figure 2c

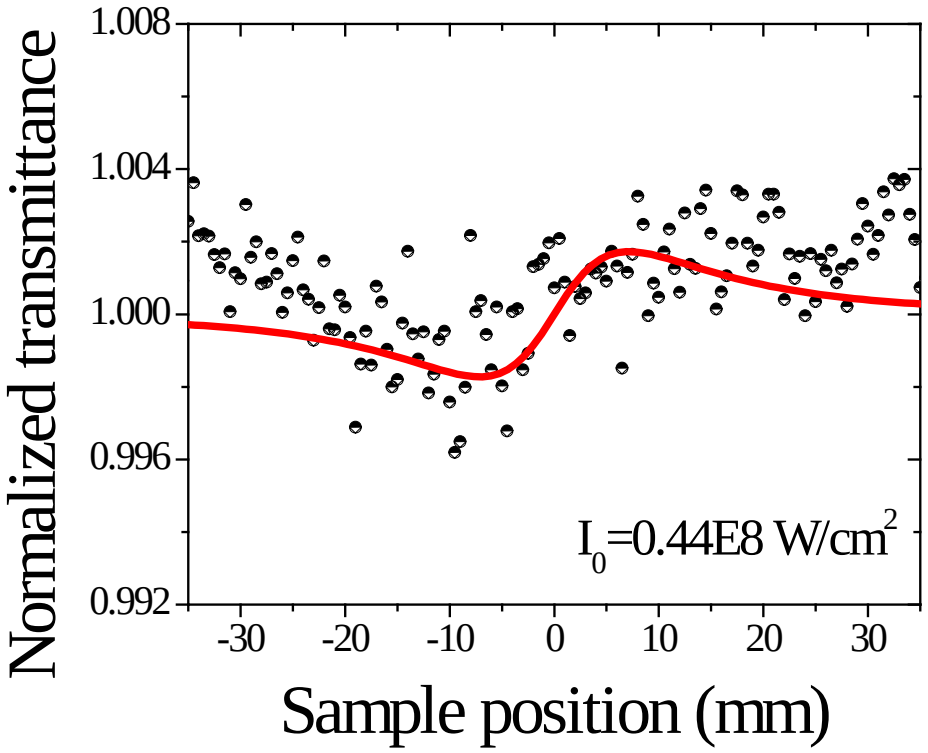
Normalized transmittance
1.008
1.004
1.000
0.996
0.992
-30
-20
-10
0
10
20
30
Sample position (mm)
I0=0.44E8 W/cm2

Figure 2d

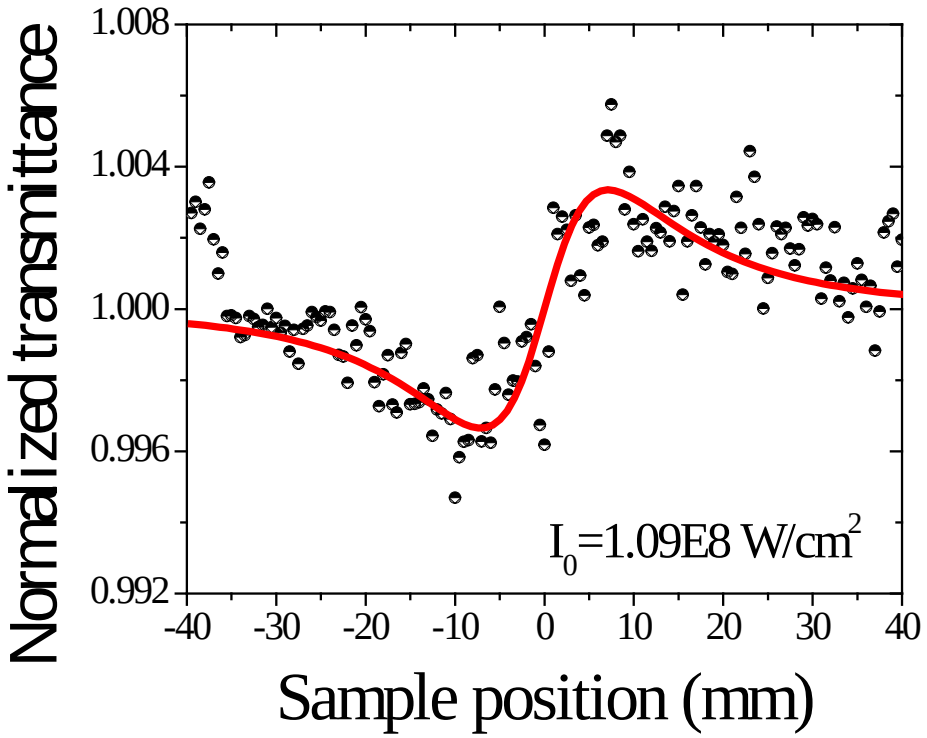
Normalized transmittance
1.008
1.004
1.000
0.996
0.992
-40
-30
-20
-10
0
10
20
30
40
Sample position (mm)
I0=1.09E8 W/cm2

Figure 3

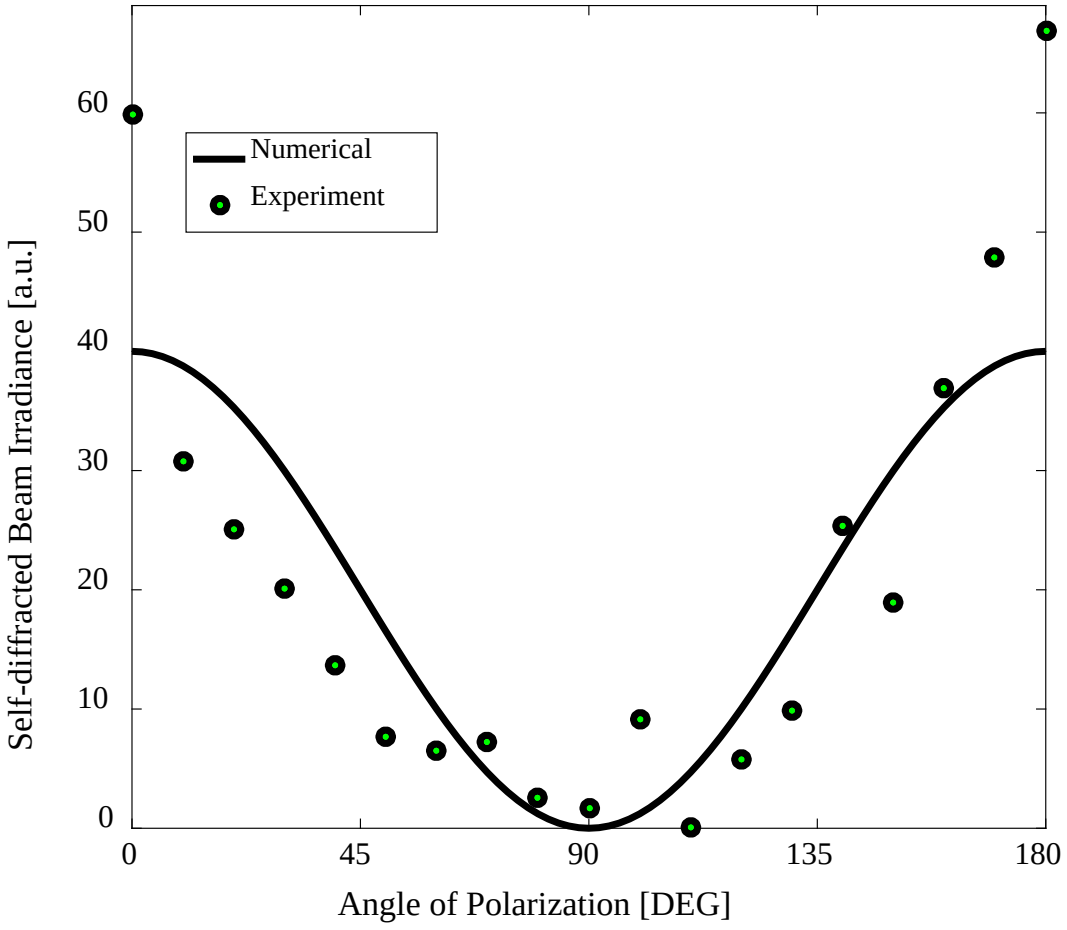
Numerical
Experiment
Self-diffracted Beam Irradiance [a.u.]
Angle of Polarization [DEG]
0
10
20
30
40
50
60
0
45
90
135
180

Figure 4

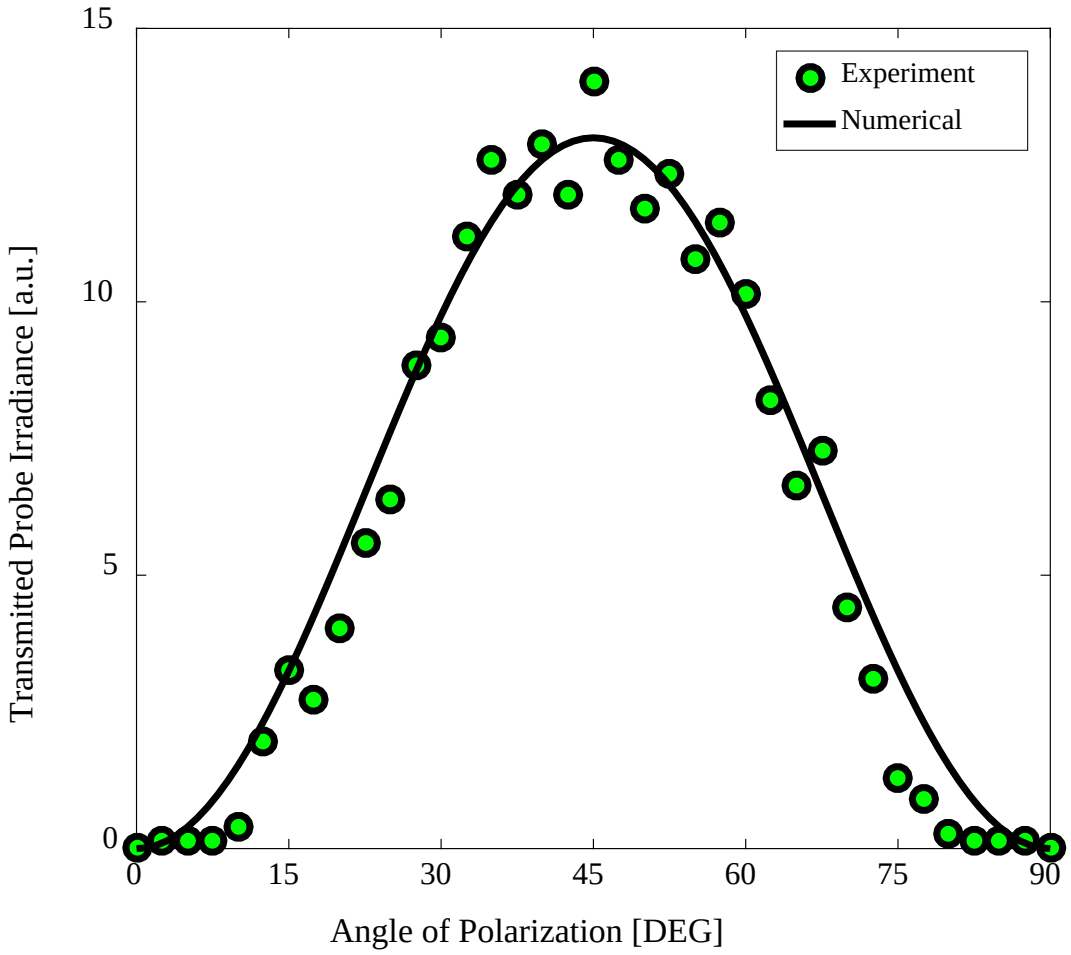
Experiment
Numerical
Transmitted Probe Irradiance [a.u.]
Angle of Polarization [DEG]
0
5
10
15
0
15
30
45
60
75
90